

Electrocatalytic Determination of Nevirapine Using a Platinum Electrode Modified with a Polymeric CoPc-Nafion-carbon nanotube Composite

Kevin Kantize, Irvin Noel Booysen*, Allen Mambanda

University of KwaZulu-Natal, School of Chemistry and Physics, Private Bag X01, Scottsville 3209, Pietermaritzburg, South Africa

*E-mail: Booyesen@ukzn.ac.za

Received: 1 February 2022/ Accepted: 4 March 2022/ Published: 7 May 2022

We report a Pt-modified electrode (*viz.* CoPc-cou-*f*-MWCNTs/Naf-5/Pt) fabricated by sequential drop casting of a nanoconjugate comprising a *tetra*-substituted coumarin cobalt phthalocyanine (CoPc-cou) and carboxylic-acid-functionalized multiwalled carbon nanotubes (*f*-MWCNTs), followed by immobilization of a 5% Nafion perfluorinated resin solution (Naf-5). Under optimized conditions, CoPc-cou-*f*-MWCNTs/Naf-5/Pt was used for the voltammetric determination of the antiretroviral drug nevirapine (NVP). The linear sweep voltammetric (LSV) response was linear from 0.6 nM to 30 μM with an estimated limit of detection (LOD) of approximately 0.2 nM, whereas the chronoamperometric response was linear over two concentration ranges. These two ranges were 4 nM to 312.5 nM (with an estimated LOD of 0.21 nM) and 2.5 μM to 30 μM. CoPc-cou-*f*-MWCNTs/Naf-5/Pt also showed excellent discriminatory sensing abilities toward selected organic contaminants. An average recovery of 110% was attained using the modified electrode for the LSV analysis of a spiked river-water sample, demonstrating the applicability of the modified electrode to accurate NVP analysis.

Keywords: metallophthalocyanine; nevirapine; coumarin; carbon nanotubes; Nafion.

1. INTRODUCTION

Human immunodeficiency virus (HIV) infection and acquired immunodeficiency syndrome (AIDS) pose severe threats to global health with dire consequences. Since the discovery of HIV, massive efforts have been expended on finding a cure. Various drugs have been approved for treatment. These drugs fall into six categories: 1) nucleotide reverse transcriptase inhibitors (NtRTIs), 2) nucleoside reverse transcriptase inhibitors (NRTIs), 3) nonnucleoside reverse transcriptase inhibitors (NN-RTIs), 4) protease inhibitors (PIs), 5) entry inhibitors (EIs), and 6) integrase inhibitors (INIs).[1] Nevirapine (NVP) is classified as a NN-RTI and is often used in tandem with other reverse transcriptase inhibitors

for effective treatment.[2] NVP inhibits the transcription of RNA into DNA by binding to a site removed from the active site of the reverse transcriptase enzyme.[3]

The Republic of South Africa (RSA) has an estimated 7.5 million people living with HIV. The RSA health care system administers one of the largest antiretroviral therapy (ART) programs in the world, which has been credited for a significant decrease in the rate of new infections, especially that of mother-to-child transmission.[4] The widespread use of antiretroviral drugs (ARVDs), as well as the challenges related to the safe disposal of these drugs in domestic wastes in most metropolitan cities, qualify ARVDs as a subclass of emerging contaminants of concern for water resources that poses a health and safety risk to end-users.[5] The occurrence of NVPs has been recently reported in river water sampled near the cities of Johannesburg and Durban.[6, 7] The prevalence of residual pharmaceutical compounds is linked to the incomplete removal of these compounds at wastewater treatment facilities, where the influent wastes have diverse origins, including medical wastes.

Various analytical techniques, including high-performance liquid chromatography (HPLC),[8, 9] gas chromatography–mass spectrometry (GC–MS),[10] ultraviolet–visible (UV–Vis) spectrometry,[11] liquid chromatography coupled to tandem mass spectrometry (LC–MS/MS),[2] and voltammetry techniques, have been developed for the accurate quantitative determination of NVP in tablet formulations and human blood plasma.[12–14] In recent years, electrochemical techniques have attracted the attention of many researchers, largely because of being affordable, sensitive, accurate and fast alternatives for the determination of various analytes. Voltammetric determination of NVP by chemically modified electrodes (CMEs) has been reported, including nanoparticles immobilized on glassy carbon (GC),[12, 15] electrodes modified with carbon nanotubes (CNTs) [16] and polymer-based electrodes.[16, 17]

Reports in the literature trends show that working electrodes modified with thin films of metallophthalocyanines (MPcs) in combination with other highly conductive materials can synergistically lower the redox overpotentials of most reactions and enhance the electrode Faradaic currents.[18–20] In particular, the conductivity of MPc-based films has been improved by incorporating graphitic-based materials (*viz.* graphene sheets, tubes and quantum dots) and metallic nanoparticles.[21–23] The incorporation of these conductivity-promoting materials enables rapid electron transfer between analytes adsorbed on the thin film and the electrode surface. In addition, CMEs based on composites of metallophthalocyanines (MPcs) and other nanoconjugates offer higher electroactive surface areas for enhanced immobilization of analytes compared to bare substrates. Consequently, modifying the surfaces of these conducting thin films increases the accessibility of catalytic sites to analytes, facilitating analyte preconcentration on CME surfaces. Unlike other porous carbon supports, the nanodimensionality, composition and robustness of carbon nanotubes enables modulation of the electrochemical properties and processability of nanoconjugate films.[24, 25]

Herein, we report the modification of a platinum electrode via drop casting of a suspension mixture of coumarin-substituted CoPc and carboxylic-acid-functionalized multiwalled carbon nanotubes, followed by drying of the resultant modified electrode at room temperature. Thereafter, a classical electron-mediating polymeric film, Nafion (Naf), was drop-cast on the CME interface. Carbon nanotubes were selected for incorporation into the immobilized thin films on the basis of intrinsic properties, including mechanical and chemical stability, as well as electrical conductivity, whereas Naf

is a perfluorinated sulfonated cation exchanger that was selected for a high permeability to cations and good chemical robustness.[22]

2. EXPERIMENTAL

2.1 Materials

Organic and inorganic precursors, 7-hydroxy-4-trifluoromethyl coumarin, 4-nitrophthalonitrile and cobalt(II) chloride, were procured from Sigma–Aldrich. The basic catalysts, 1,8-diazabicyclo[5.4.0]undec-7-ene (DBU) and potassium carbonate, that were used to synthesize the compounds; electrochemical-grade supporting electrolyte, tetrabutylammonium tetrafluoroborate (TBABF₄); carboxylic-acid-functionalized multiwalled carbon nanotubes (*f*-MWCNTs, 8% carboxylic-acid-functionalized, average diameter x *length*: 9.5 nm x 1.5 nm) and Nafion (Naf) perfluorinated resin solution) were acquired from the same company.

Organic solvents and other materials, including phosphorous pentoxide, molecular sieves (4 Å), silicon dioxide for column chromatography and silica plates for thin layer chromatography, were all purchased from Merck SA. Dimethylformamide (DMF) was dried and stored over molecular sieves, and ultrapure water was produced using an Elga Purelab Ultra system. The derivatized phthalonitrile, 4-(4-trifluoromethyl)-coumarin-7-oxy) phthalonitrile, and the corresponding CoPc, β -tetra(7-oxy-4-trifluoromethylcoumarinphthalocyaninato)Co(II) *viz.* CoPc-cou, were synthesized using a method we have previously reported.[23]

2.2 Equipment

Spectroscopic data for the metal complex were collected on a Bruker Alpha FTIR spectrometer, a 400-MHz Bruker NMR spectrometer and a Perkin-Elmer Lambda 25 UV–Vis spectrophotometer. The nominal mass of CoPc-cou was measured using a Waters Micromass LCT Premier MS instrument equipped with an electrospray ionization (ESI) source and a time-of-flight (TOF) mass analyzer. Elemental analysis data were collected using a CHNS-O Flash 2000.

An Autolab PGSTAT 302N electrochemical workstation with electrochemical impedance spectroscopy (EIS) capabilities was used to conduct voltammetry and EIS experiments. The EIS data were fitted using various circuits in the Autolab NOVA 1.7 software bundle. Electroanalytical experiments were performed using a conventional system comprising a platinum working electrode, with an Ag|AgCl wire and Pt rod as the counter and pseudo reference electrodes, respectively. A Metrohm 827 pH meter (Switzerland) was regularly calibrated before being used to measure the pH.

The platinum electrode surface had a diameter of 5 mm (with a cross-sectional area of approximately 0.20 cm²) and was refreshed on a Buehler-felt pad using 0.5- μ m alumina paste and subsequently washed with ultrapure water. Thereafter, the electrode was placed in an ultrasonic bath containing acetone for 5 minutes and rinsed again with ultrapure water. Various chemically modified electrodes were prepared and tested to identify modifiers that promote electrocatalytic activity.

2.3 Electrode modification

A 1 mM solution of CoPc-cou in dried DMF was electropolymerized on a Pt surface to yield a CoPc-cou-Pt electrode.[23] The CME was further modified by the drop-dry method using a 5% Nafion (Naf-5) solution to yield a CoPc-cou/Naf-5/Pt electrode. The resulting electrode was dried at room temperature. Next, the following three variants of the CoPc-cou/Naf-5/Pt electrode were fabricated. The first variant, Naf-5/Pt CME, was prepared by modifying the bare Pt electrode with Naf-5 alone using the drop-dry method (at room temperature). A CoPc-cou-*f*-MWCNTs/Naf-5/Pt electrode was similarly fabricated by a sequential process. That is, CoPc-cou was premixed with 0.5 mg of CoPc and 1 mg of *f*-MWCNTs in dry DMF under ultrasonication for one hour to generate a nanoconjugate mixture. The mixture was drop-cast onto a bare Pt electrode and allowed to dry at room temperature. To ensure robustness, the nanoconjugate film was further immobilized by drop casting of Naf-5, followed by drying at room temperature. The third variant (*viz.* *f*-MWCNTs-Naf-5/Pt) was fabricated from a film of *f*-MWCNTs dispersed in a Naf-5 solution. The suspension was ultrasonicated for 30 minutes and immobilized on a Pt electrode surface, followed by drying at ambient temperature to render the fourth CME.

3. RESULTS AND DISCUSSION

3.1 Electrochemical responsiveness of CMEs

To evaluate the analytical sensitivity and electrocatalytic oxidation behavior of the electrodes toward NVP, oxidation peak currents (I_{pa}) and oxidation peak potentials E_{pa} were extracted from the cyclic voltammograms (CVs) obtained for the bare electrode and four CMEs placed in a 0.1 M phosphate-buffered saline (PBS) containing 100 μ M NVP. The peak current was corrected for the background current (see Figure 1 and Table 1).

A chemically modified electrode should be constructed for selective and sensitive detection of a specific analyte in a multifarious real sample while ensuring that the electron-mediating surface remains robust over multiple analysis cycles. Consequently, we assessed the electrocatalytic behaviors of the different CMEs in an analyte solution of 100 μ M NVP in phosphate-buffered saline (PBS) (see Figure 1). Table 1 shows the NVP oxidation peak currents and potentials determined from the CVs for the bare electrode, the CMEs containing the commercially available polymeric Naf-5 film and the CME containing CoPc-cou were not discernible. However, incorporating *f*-MWCNT into the framework of *f*-MWCNTs-Naf-5/Pt and CoPc-cou-*f*-MWCNTs/Naf-5/Pt produced CMEs with substantially higher oxidation peak currents and lower oxidation potentials. For instance, the Faradaic current of CoPc-cou-*f*-MWCNTs/Naf-5/Pt was approximately 225 times higher than that of the bare Pt electrode.

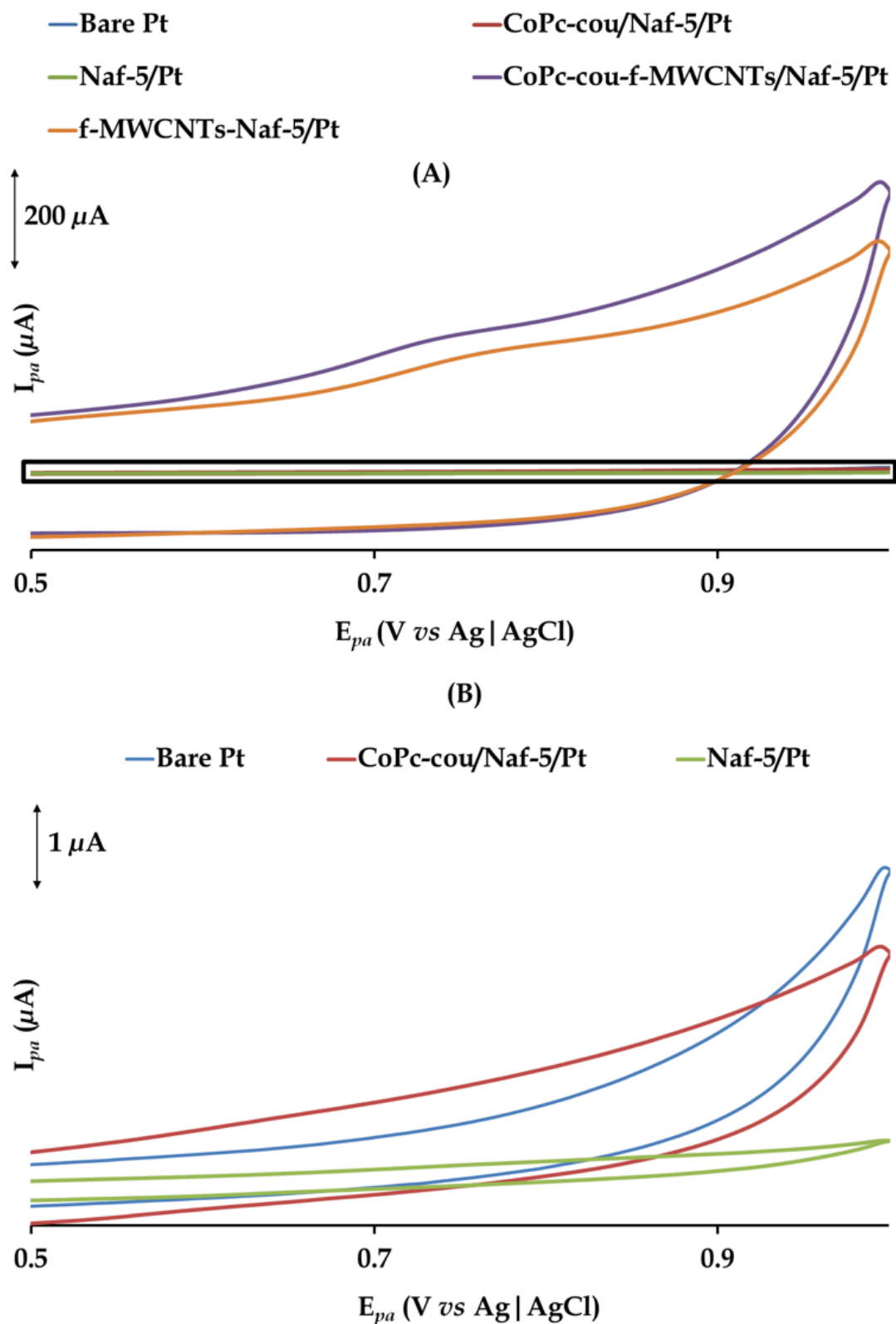


Figure 1. (A) CVs obtained for bare Pt, CoPc-cou/Naf-5/Pt, Naf-5/Pt, CoPc-cou-f-MWCNTs/Naf-5/Pt and f-MWCNTs-Naf-5/Pt in an aqueous solution of 100 μM NVP in 0.1 M PBS (pH = 12). (B) Magnified CVs enclosed by the black rectangle in (A) obtained for bare Pt, CoPc-cou/Naf-5/Pt and Naf-5/Pt.

Table 1. Nevirapine peak currents and redox potentials (V vs. Ag|AgCl) obtained using different electrodes.

Pt electrode	I_{pa} (μA) ¹	E_{pa} (V)
Bare Pt	nd ²	nd ²
Naf-5/Pt	nd ²	-nd ²
CoPc-cou/Naf-5/Pt	nd ²	nd ²
<i>f</i> -MWCNTs- Naf-5/Pt	30	0.742
CoPc-cou- <i>f</i> -MWCNTs/Naf-5/Pt	36	0.690

¹ Peak currents corrected for background current.

² Not distinguishable (peak currents and potentials are not discernible).

The best electroanalytical response was obtained for the Pt electrode modified by drop casting a suspension solution mixture of CoPc-cou and *f*-MWCNTs, followed by immobilization of a Naf-5 drop. The resultant CME, CoPc-cou-*f*-MWCNTs/Naf-5/Pt, exhibited a higher electrocatalytic current and a lower redox potential than the other electrodes. This remarkable trend is attributed to the synergetic effect between the CoPc-cou-*f*-MWCNTs nanoconjugate constituents and Nafion (5%), which facilitates electronic mediation between the bulk analyte solution and the Pt substrate.

3.2 The effect of pH

Figure 2A shows the influence of the pH on the electrooxidation of 100 μM NVP by CoPc-cou-*f*-MWCNTs/Naf-5/Pt over the 6–12 pH range. The CVs show that over this pH range, the capacitance-corrected peak currents increased, while the peak potentials shifted negatively in tandem. However, no NVP oxidation signals were detected for pHs < 6 (see Figures 2A and 2B). This lack of response occurred because acidic media shift the reaction equilibrium to the left (see Scheme 1).[16] The electro-oxidation of NVP was optimal at a pH of 12, which was used for the remainder of the electrocatalytic studies. The slope value of 0.054 V indicated an equal number of protons and electrons participated in NVP oxidation, which is consistent with the $2e^-/2H^+$ electro-oxidation reaction of NVP (see Figure 2C).

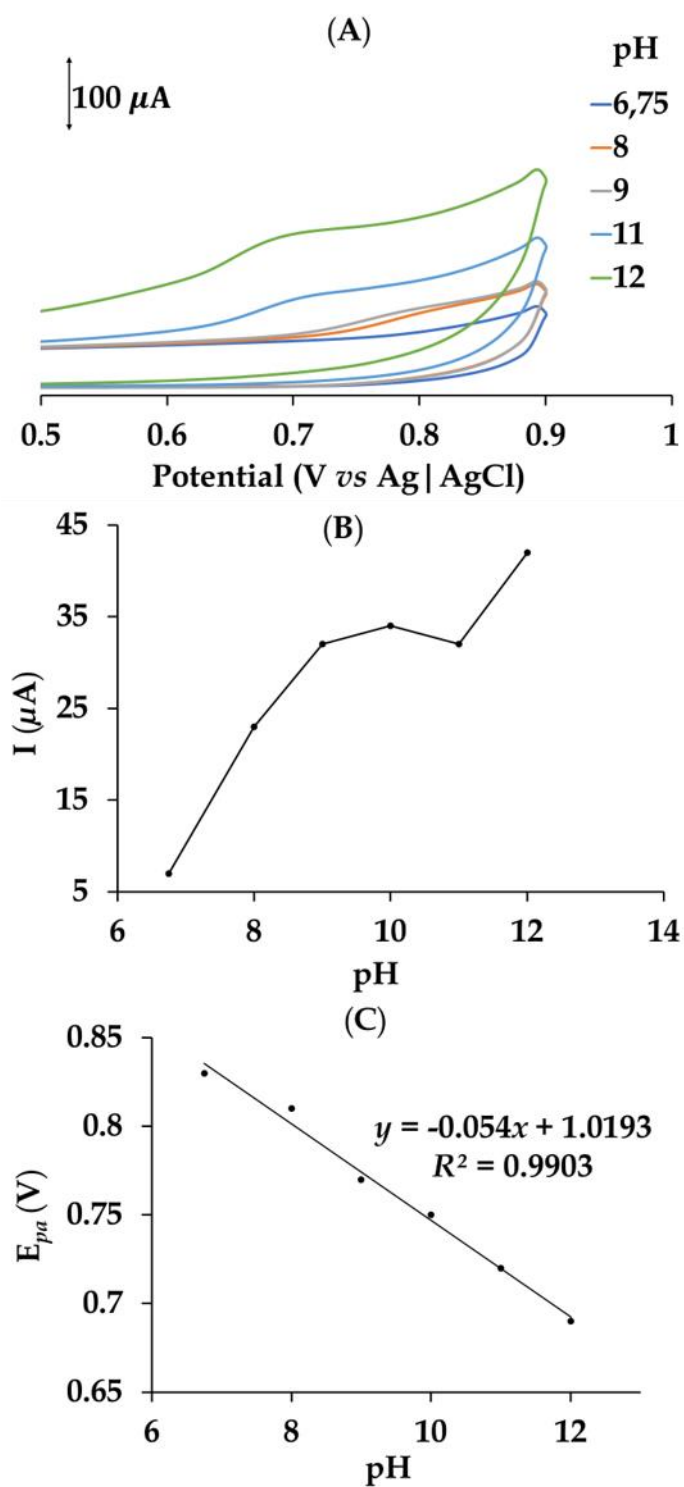
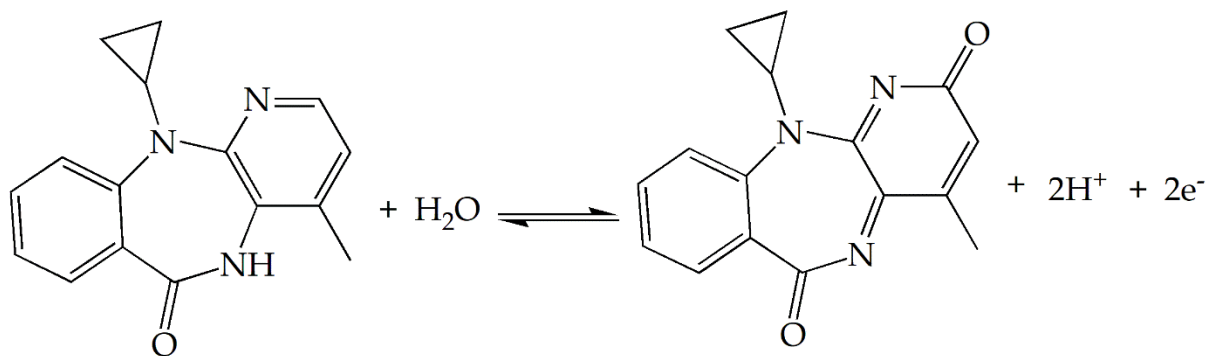


Figure 2. (A) CVs obtained using CoPc-cou-f-MWCNTs/Naf-5/Pt placed in 100 μM NVP in PBS with different pHs, (B) I_{pa} vs. pH, and (C) E_{pa} vs. pH.



Scheme 1. Redox interconversion of NVP at pH 12.

3.3 The effect of the scan rate

To further elucidate the mechanism of NVP oxidation, the effect of the scan rate was explored over the range of 25 to 250 mV/s using a PBS (0.1 M, pH 12) buffer containing 100 μ M NVP (see Figure 3A). The peak currents were linear in both the square root of the scan rates and the scan rates, indicating both diffusion and adsorption mass transport processes occurred (see Figures 3B and 3C). A plot of the logarithm of peak currents ($\text{Log } I_{pa}$) versus the logarithm of the scan rate ($\text{Log } \nu$) had a slope of 0.5735, which lies within the 0.5 to 1 range, corroborating that both adsorption and diffusion mass transport processes play integral roles in the NVP oxidation mechanism (see Figure 3D).[17] However, the plot shown in Figure 3C has a higher regression coefficient than that shown in Figure 3B, indicating that the oxidation process is largely adsorption-controlled. Based on the Laviron method,[26] the peak potential (E_{pa}) can be related to the logarithm of the scan rate ($\text{Log } \nu$) of an irreversible system as given below.

$$E_{pa} = E^0 + \left(2.303 \frac{RT}{(1-\alpha)nF}\right) \text{Log} \left(\frac{RTk^0}{(1-\alpha)nF}\right) + \left(2.303 \frac{RT}{(1-\alpha)nF}\right) \text{Log } \nu \quad (1)$$

In the equation presented above, α is the charge-transfer coefficient, ν is the scan rate, n is the number of transferred electrons and k^0 is the standard reaction rate constant. The slope of the E_{pa} vs. $\text{Log } \nu$ plot (Figure 3E) was used to determine an α of 0.545, which is close to that of 0.5 for an irreversible system. The Tafel slopes, as defined in Equation (1), were calculated from the plot of the peak potential (E_{pa}) vs. the logarithm of the scan rate ($\text{Log } \nu$). The Tafel slope of 130 mV is higher than the typical range of 30–120 mV/decade and confirms the strong interaction between the substrate and the thin film on the electrode.[27] The abovementioned mechanistic data shows that the analyte diffuses easily to the CME interface to undergo adsorption and subsequent electro-oxidation. NVP adsorption onto the CME surface may be governed by intermolecular interactions of NVP with the coumarin moieties appended to the CoPc core, the sulfonic groups of the Nafion conducting polymer and the carboxylic acid groups of the *f*-MWCNTs.

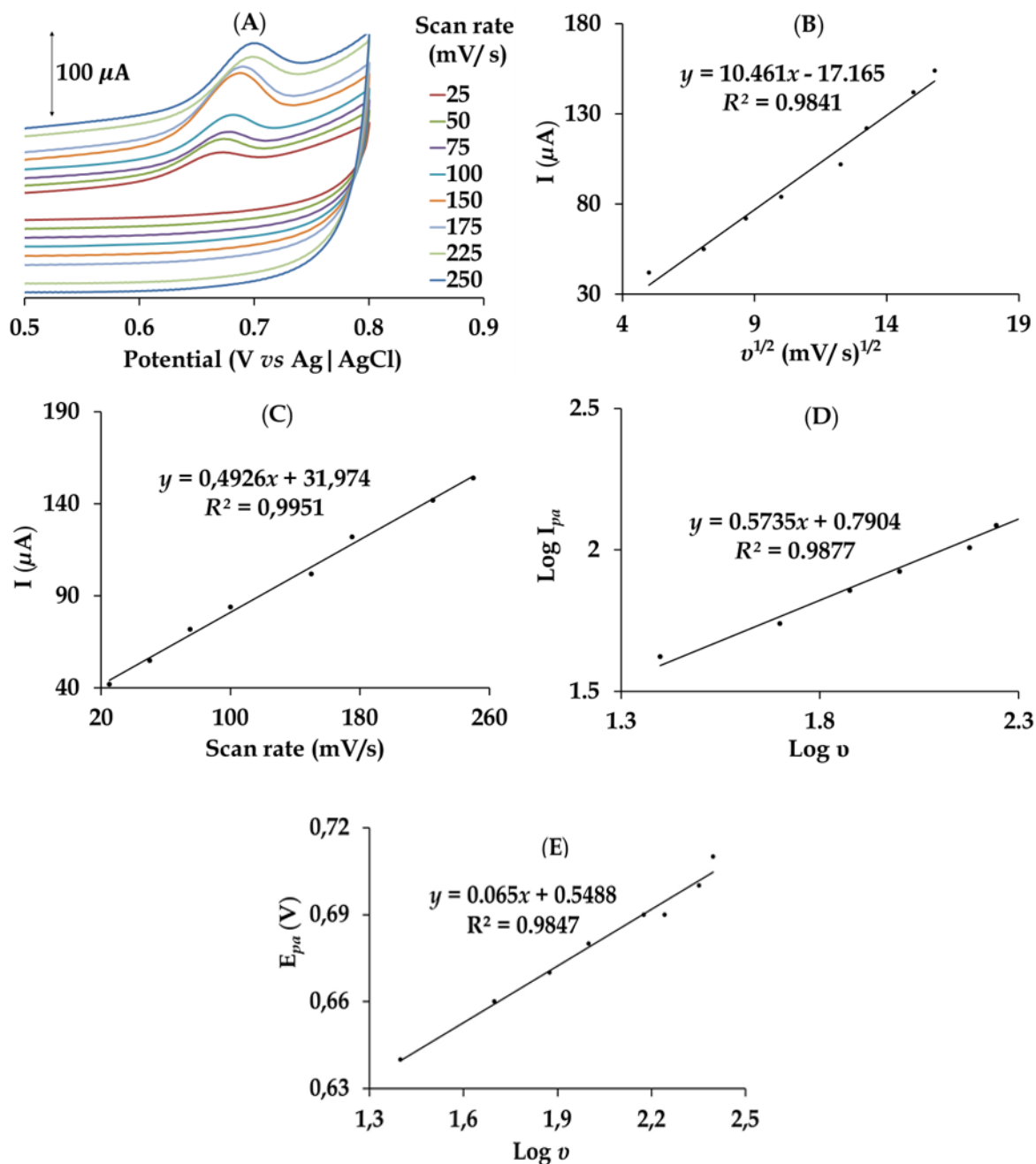


Figure 3. (A) CVs obtained at various scan rates (mV/s) using CoPc-cou-f-MWCNTs/Naf-5/Pt placed in 100 μ M NVP in PBS (pH = 12), (B) I_{pa} vs. the square root of the scan rate, (C) the anodic peak current vs. the scan rate, (D) $\text{Log } I_{pa}$ vs. $\text{Log } v$ and (E) E_{pa} vs. $\text{Log } v$.

3.4 Surface area and coverage

The surface area is an important measure of the electrocatalytic efficacy of a CME. Therefore, a redox probe solution of $\text{K}_3[\text{Fe}(\text{CN})_6]$ was used to determine the effective CME surface area. Figure 4A shows the CVs obtained at different scan rates using CoPc-cou-f-MWCNTs/Naf-5/Pt placed in 5 mM $\text{K}_3[\text{Fe}(\text{CN})_6]$ prepared in an aqueous solution of 0.1 M KCl.

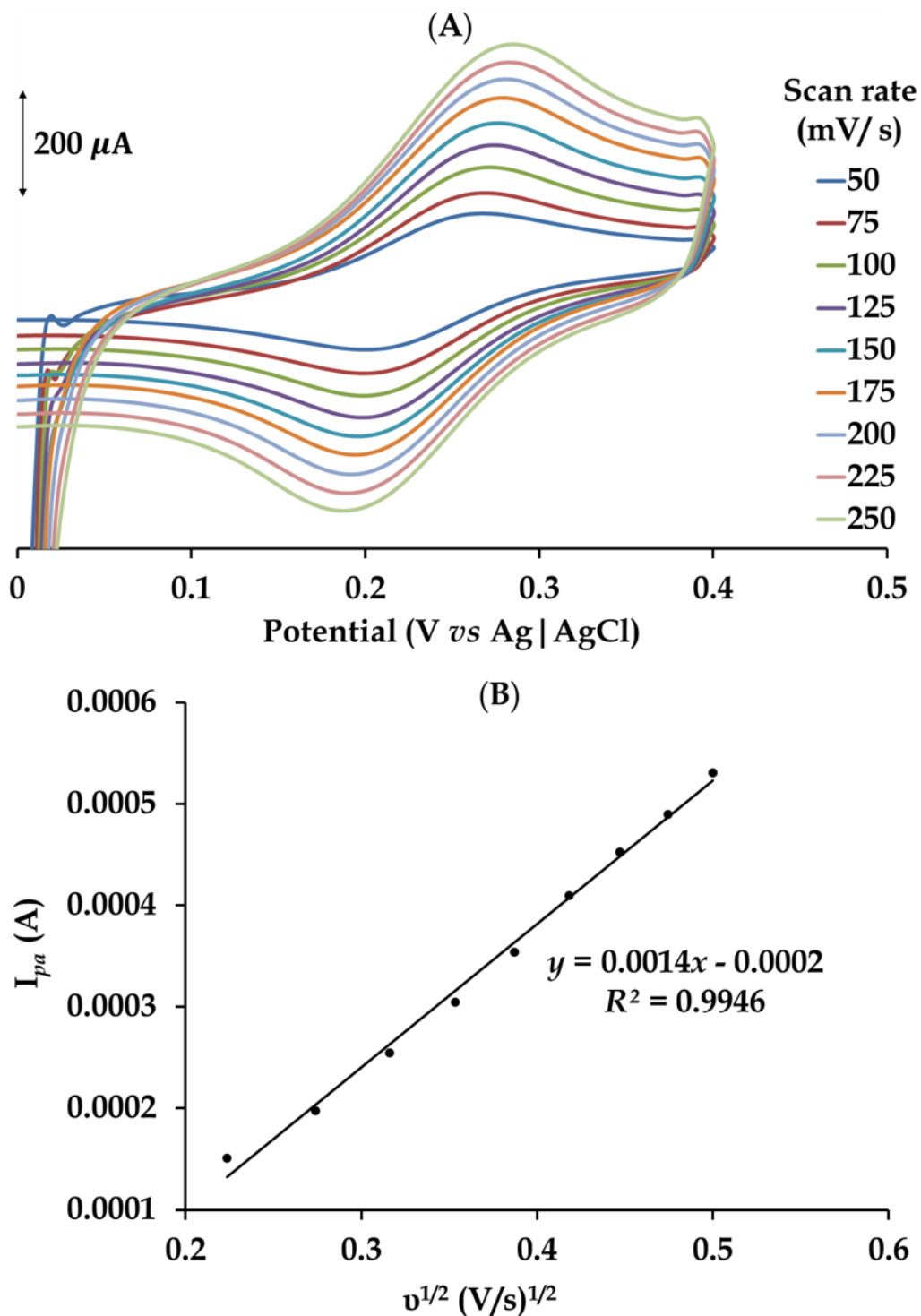


Figure 4. (A) CVs obtained at different scan rates (50, 75, 100, 125, 150, 175, 200, 225, and 250 mV/s) using CoPc-cou-f-MWCNTs/Naf-5/Pt placed in 5.0 mM $K_3[Fe(CN)_6]$ prepared from 0.1 M KCl (aq) at pH 12. (B) I_{pa} vs. the square root of the scan rate.

The effective surface area of the fabricated CME was determined using the Randles-Sevcik equation (Equation 2):[28]

$$I_{pa} = 2.69 \times 10^5 AD^{1/2} n^{3/2} \nu^{1/2} C \tag{2}$$

where A is the effective surface area, D is the diffusion coefficient of $K_3[Fe(CN)_6]$, v is the scan rate, C is the $K_3[Fe(CN)_6]$ bulk concentration, and n is the number of transferred electrons ($n = 1$). The slope of the plot of the oxidation peak current against the square root of the scan rate was used to calculate the effective surface area (see Figure 4B). The relative effective CME surface area of 0.41 cm^2 is significantly higher than that of the bare Pt electrode and confirms that electrode modification increases the number of sites available for analyte adsorption.

To further characterize the modified electrode, the CME surface coverage was calculated using the obtained effective surface area and the total charge under the peak using Equation (3):

$$\Gamma = \frac{Q}{nFA} \quad (3)$$

where Γ is the surface coverage, n is the number of transferred electrons, F is the Faraday constant and A is the effective surface area. The surface coverage value of $5.47 \times 10^{-10} \text{ mol cm}^{-2}$ exceeds the value of $1 \times 10^{-10} \text{ mol.cm}^{-2}$ for a Pc molecule lying flat on the electrode.[29]

3.5 Electrochemical impedance spectroscopy (EIS)

EIS experiments were conducted over a frequency range of 0.1 Hz to 100 kHz. Figure 5D shows the electrical circuit that was fitted to the impedance spectra. The kinetic (R_{ct}) and diffusion (Z_w) parameters are both associated with mixed electrode reactions. All the impedance spectra, except for the that of unmodified Pt electrode, are composed of a depressed semicircle in the high-frequency range and a straight line in the low-frequency range (see Figures 5A – C). The high-frequency arc is well-known to indicate charge transfer limitations that can be directly quantified in terms of the semicircle diameter, whereas the straight line is characteristic of diffusion systems (refer to Table 2).[30, 31]

In the results summarized in the table, CoPc-cou-*f*-MWCNTs/Naf-5/Pt has an R_{ct} of 195Ω , indicating excellent interfacial charge-transfer capability. The bare electrode has a higher R_{ct} ($1.01 \text{ k} \Omega$), and therefore a higher resistance to charge transfer, than the CMEs. The fast charge-transfer kinetics unequivocally result from the collective activity of the CoPc core, *f*-MWCNTs and Naf-5 polymer. The aforementioned trend further corroborates the electrocatalytic data obtained by cyclic voltammetry shown in Figure 1.

Note that the values of n (an exponent related to the depression angle) are less than 1 for all the CMEs, indicating non-homogeneity of the CME surfaces.[32] The phase angles in the Bode plots were $\sim 70^\circ$ for the bare Pt electrode compared to $\sim 2^\circ$ and $\sim 3^\circ$ for the CoPc-cou-*f*-MWCNTs/Pt and CoPc-cou-*f*-MWCNTs-Naf-5/Pt electrodes, respectively (see Figure 6). These phase angles are less than the 90° value for an ideal capacitor, which further confirms the noncapacitive nature of the electrodes.

Table 2. Summary of EIS data collected using the bare and modified working electrodes in 5 mM $[\text{Fe}(\text{CN})_6]^{3-/4-}$. The errors are shown in brackets.

Pt	R_s (Ω)	R_{ct} (Ω)	Z_w (mS)	$^a n$
Bare	15.1 (0.6)	1010 (1)	0.8 (1.5)	-
CoPc-cou-f-MWCNTs	25.1 (0.4)	329 (7)	9.88 (4.4)	0.6 (0.5)
CoPc-cou-f-MWCNTs/Naf-5	20.2 (0.6)	195 (5)	4.6 (6.8)	0.7 (0.4)

^a The exponent n is related to the depression angle.

The percent errors are obtained from fitting the experimental Nyquist plot are shown in brackets.

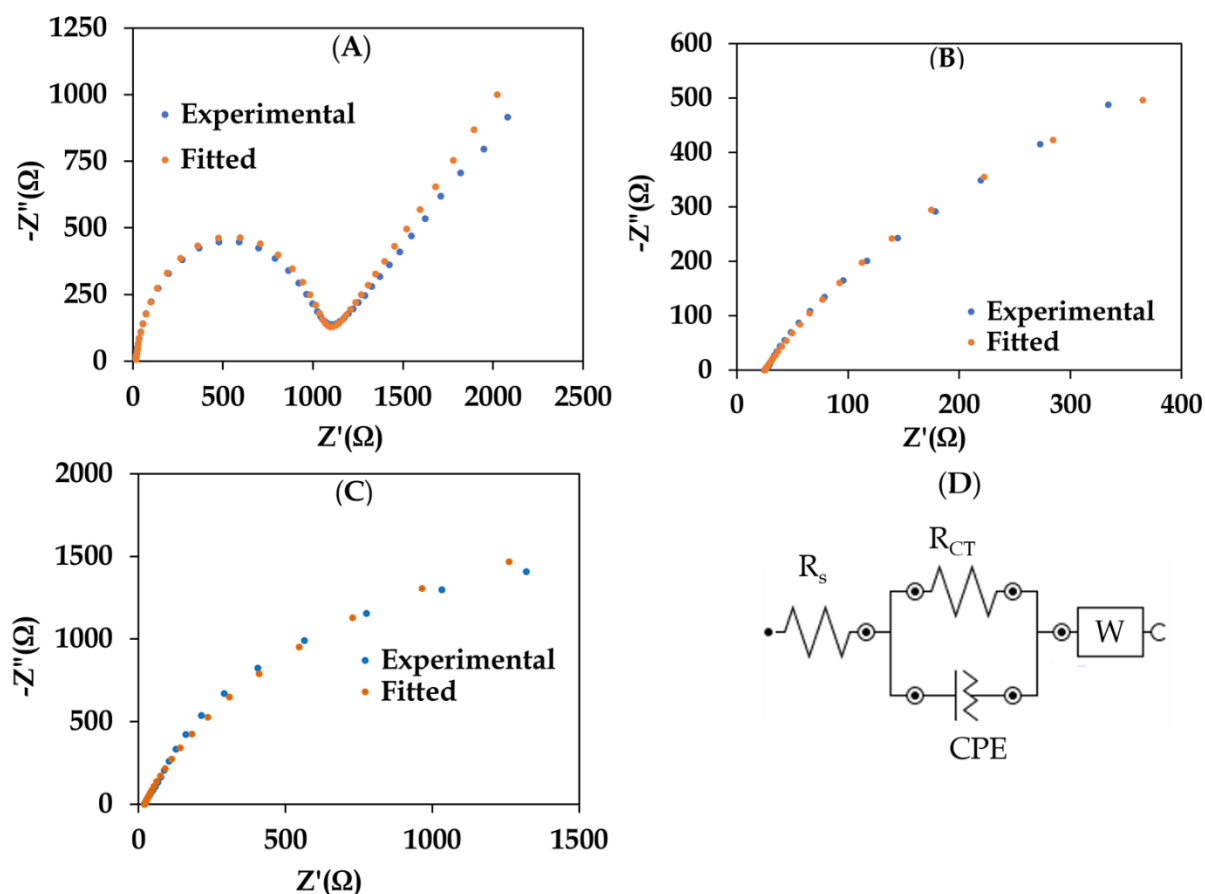


Figure 5. Nyquist plots obtained for a solution of 5 mM $[\text{Fe}(\text{CN})_6]$ prepared in PBS using the (A) bare Pt electrode, (B) CoPc-cou-f-MWCNTs/Pt electrode and (C) CoPc-cou-f-MWCNTs/Naf-5/Pt electrode. (D) The equivalent circuit used to fit the EIS data.

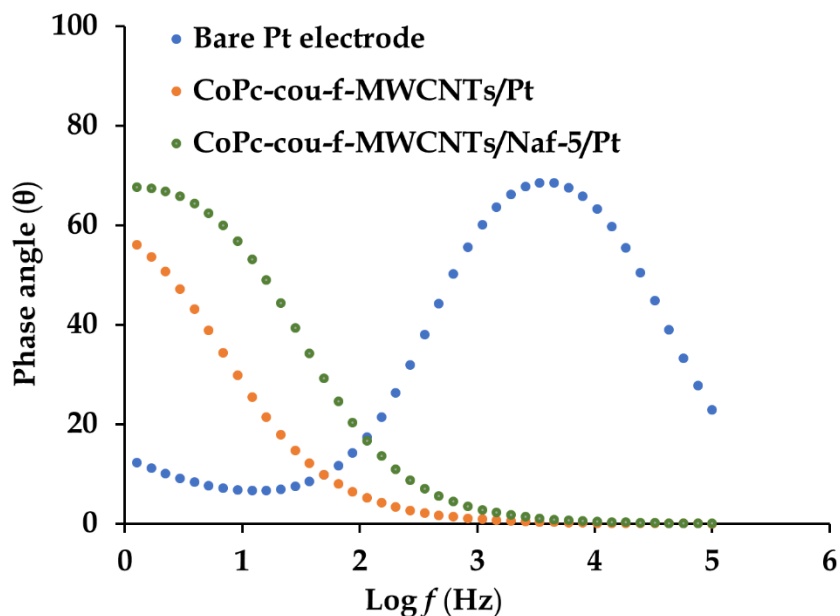


Figure 6. Bode plots generated for different working electrodes.

3.6 Redox reaction kinetics

Single-step chronoamperometry was used to determine the electrocatalytic rate constant using CoPc-cou-f-MWCNTs/Naf-5/Pt in 100 μM NVP in PBS (pH = 12) under diffusion-controlled experimental conditions (see Figure 7A). The chronoamperomogram of the CME was obtained by applying overpotentials with respect to the E_{pa} of NVP at 0.68 V obtained from the corresponding CVs over an interval of 7–15 s. The rate constant for the oxidation reaction of NVP was determined using Equation (4):[33]

$$\frac{I_c}{I_b} = \gamma^{1/2} \pi^{1/2} = \pi^{1/2} (kCt)^{1/2} \quad (4),$$

where I_c and I_b are the currents in the presence and absence of NVP, respectively; k is the catalytic rate constant ($\text{M}^{-1} \text{s}^{-1}$); C is the nevirapine bulk concentration; and t is the elapsed time in seconds. The diffusion-controlled rate constant was calculated from a plot of I_{cat}/I_{buff} vs. $t^{1/2}$ (see Figure 7B). The diffusion rate constant of $9.68 \times 10^4 \text{ M}^{-1} \text{ s}^{-1}$ is higher than reported chronoamperometric rate constants for NVP and a bioanalyte, dopamine.[14, 34, 35] NVP and dopamine detection proceed by similar oxidative mechanisms, and our CME exhibits faster electron transfer kinetics ($> 10^3 \text{ M}^{-1} \text{ s}^{-1}$) than the modified electrodes used for dopamine oxidation. Rate constants on the same order were determined for our CME and a GCE modified with a nanohybrid comprised of TiO_2 nanoparticles and graphene nanoribbons. Therefore, it is evident that the constituents of our CME electron-mediating thin film enhance the diffusion, adsorption and subsequent oxidation of NVP.

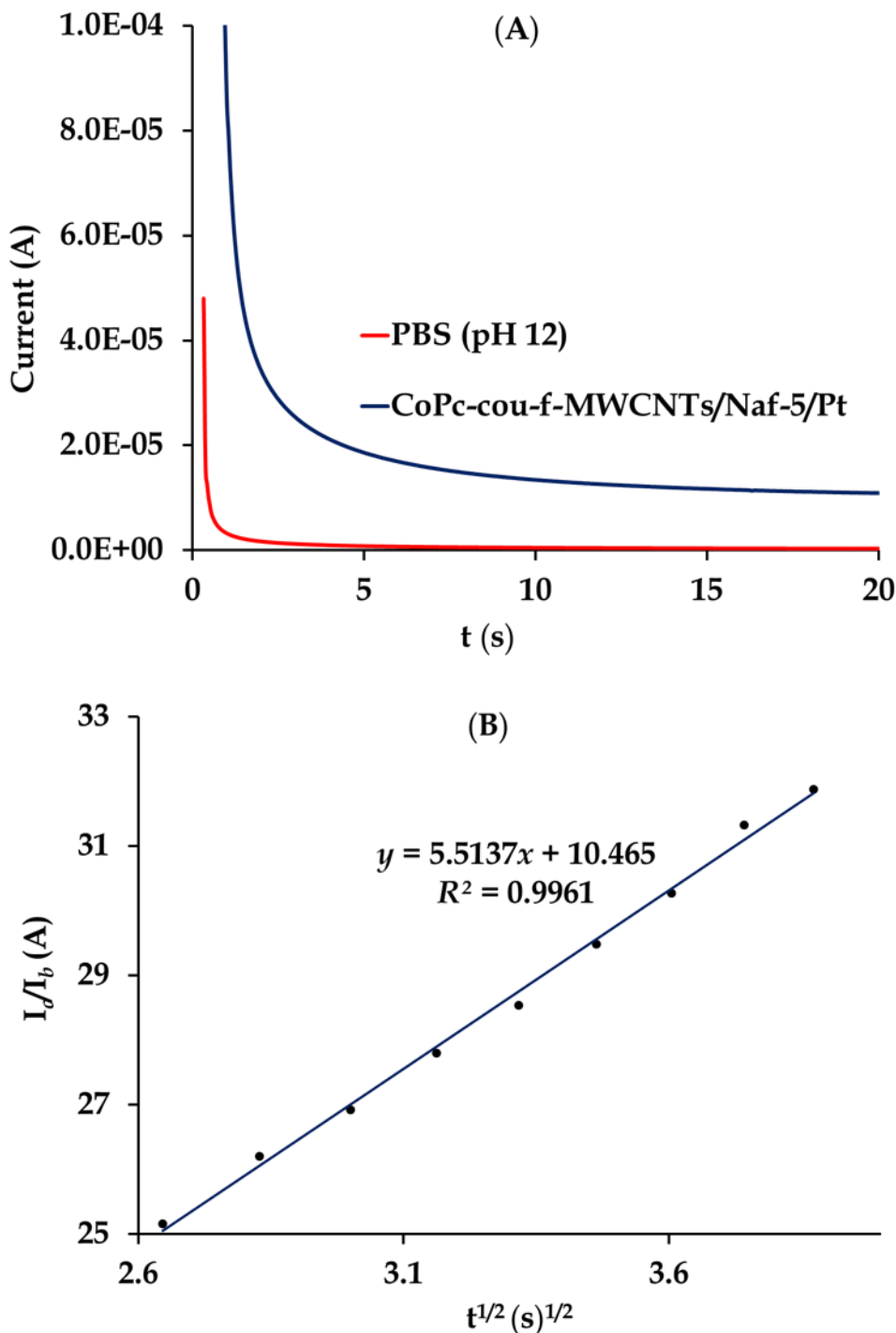


Figure 7. (A) Chronoamperograms obtained using CoPc-cou-f-MWCNTs/Naf-5/Pt placed in 100 μ M NVP prepared in a pH 12 PBS buffer. (B) $\frac{I_c}{I_b}$ vs. $t^{1/2}$.

Electrocatalytic oxidation of NVP was carried out under convective transfer conditions generated by a rotating disk electrode at variable rotation speeds (ω) to determine the heterogeneous electron transfer rate constant, k . The linear sweep voltammograms (LSVs) obtained at 10 mV/s are shown in Figure 8A. The limiting current (I_L) data were linear in $\omega^{1/2}$ according to the Levich equation:[36]

$$I_L = 0.62nFAD^{2/3}\nu^{-1/6}\omega^{1/2}C_0 \quad (5)$$

where D is the NVP diffusion coefficient, A is the electrode area, ν is the kinematic viscosity, ω is the rotation rate and C_0 is the analyte bulk concentration.

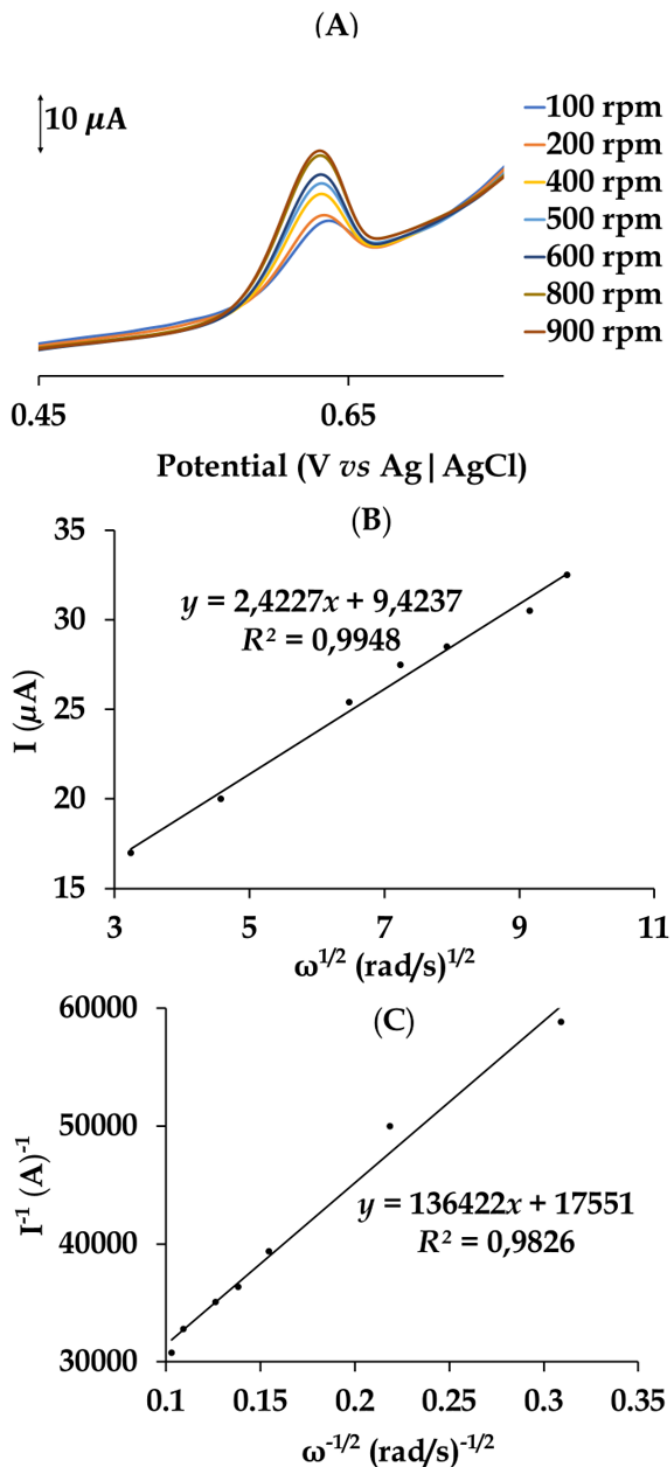


Figure 8. (A) LSVs obtained at a scan rate of 10 mV/s using CoPc-cou-f-MWCNTs/Naf-5/Pt placed in a sample of 30 μ M NVP prepared in PBS at pH 12. (B) Levich plot. (C) Koutecky-Levich plot.

Thus, the mass transfer of NVP to the surface of the disk electrode was dominated by convection currents under the experimental conditions. The data was fit to the Koutecky-Levich equation[37] given below to calculate k ($M^{-1}s^{-1}$) for the electrocatalytic oxidation of NVP at the RDE.

$$\frac{1}{I_L} = \frac{1}{nFAC_0k\Gamma} + \frac{1}{0.62nFAD^{2/3}\nu^{-1/2}C_0\omega^{1/2}} \quad (6)$$

The inverse plateau current (I_L)⁻¹ was linear in the inverse rotation speed of the electrode ($\omega^{-1/2}$) (see Figure 8C). The y-intercept of the plot yielded a rate constant of $4.4 \times 10^4 M^{-1} s^{-1}$ for the oxidation of NVP at the interface of CoPc-cou-*f*-MWCNTs/Naf-5/Pt, which is comparable to that for the diffusion-controlled process determined using the same CME.

3.7 Determination of analytical parameters

Table 3 shows the analytical parameters of CoPc-cou-*f*-MWCNTs/Naf-5/Pt determined under the predetermined optimized conditions. A comparative analysis of the linear sweep voltammetry and chronoamperometry results was used to generate calibration curves for NVP. Figure 9A shows the linear sweep voltammogram responses obtained at a fixed rotation speed of 100 rpm and scan rate of 10 mV/s using aliquots with different NVP concentrations. The electrocatalytic oxidation current increased linearly with the NVP concentration, as given by Equation (7).

$$I = 1.9958[NVP]_{\mu M} + 19.021, R^2 = 0.981 \quad (7)$$

The calibration curve was linear over a wide concentration range from 0.6 nM to 30 μM in PBS at pH 12 with a regression coefficient of $R^2=0.981$ (see Figure 9B). The standard deviation for 10 repeated measurements of a blank electrolyte solution (S_x) was used to calculate the limit of detection $LOD = 3S_x/m$ from the calibration curve as 0.2 nM.

Figure 10A shows the chronoamperometric responses obtained for different NVP concentrations. The following two linear calibration curves (Equations (8) and (9)) were obtained for CoPc-cou-*f*-MWCNTs/Naf-5/Pt.

$$I = 0.5501[NVP]_{\mu M} + 0.56822, R^2 = 0.994 \quad (8)$$

$$I = 7.0192[NVP]_{\mu M} + 3.4868, R^2 = 0.9933 \quad (9)$$

The concentrations were linear within the ranges of 0.004–0.3125 μM and 2.5–30 μM in PBS at pH 12, with regression coefficients of $R^2=0.9933$ and 0.9944, respectively (see Figures 10B and 10C). An LOD of 0.21 nM was obtained using the equation for the LOD presented above, where S_x is the standard deviation for 8 repeated measurements in PBS (pH = 12) and m is the slope of the calibration curve. As the linear sweep voltammetry data afforded a broader linear range of detection, this electroanalytical technique was chosen for subsequent analysis. Additionally, a comparative analysis of

CoPc-cou-*f*-MWCNTs/Naf-5/Pt with other reported CMEs used for the electrocatalytic detection of NVP indicates that CoPc-cou-*f*-MWCNTs/Naf-5/Pt has a higher sensitivity than other CMEs.

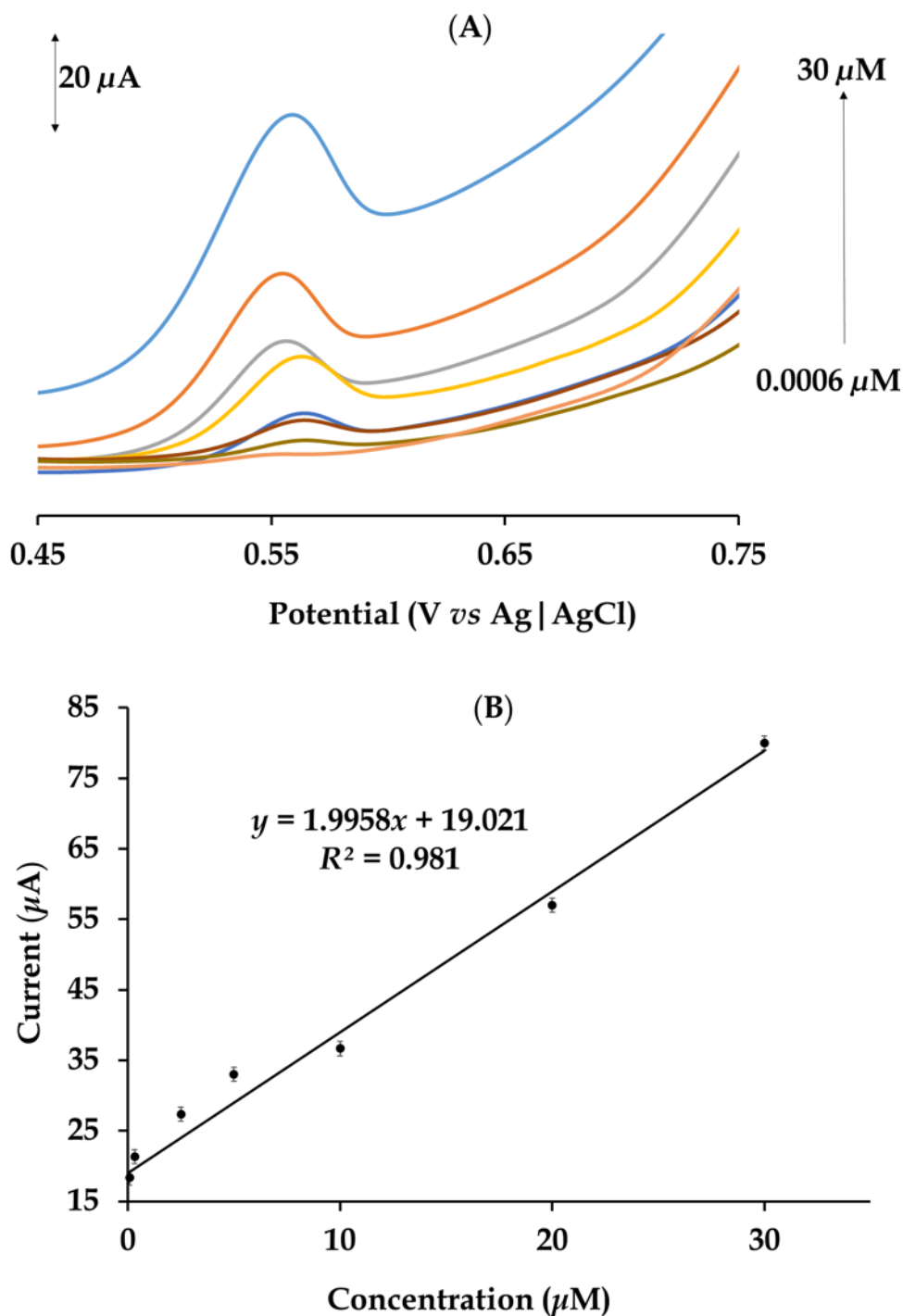


Figure 9. (A) Linear sweep voltammograms (LSVs) recorded using CoPc-cou-*f*-MWCNTs/Naf-5/Pt placed in varying concentrations of NVP prepared in PBS (pH = 12). (B) Calibration curve for the current response against the NVP concentration.

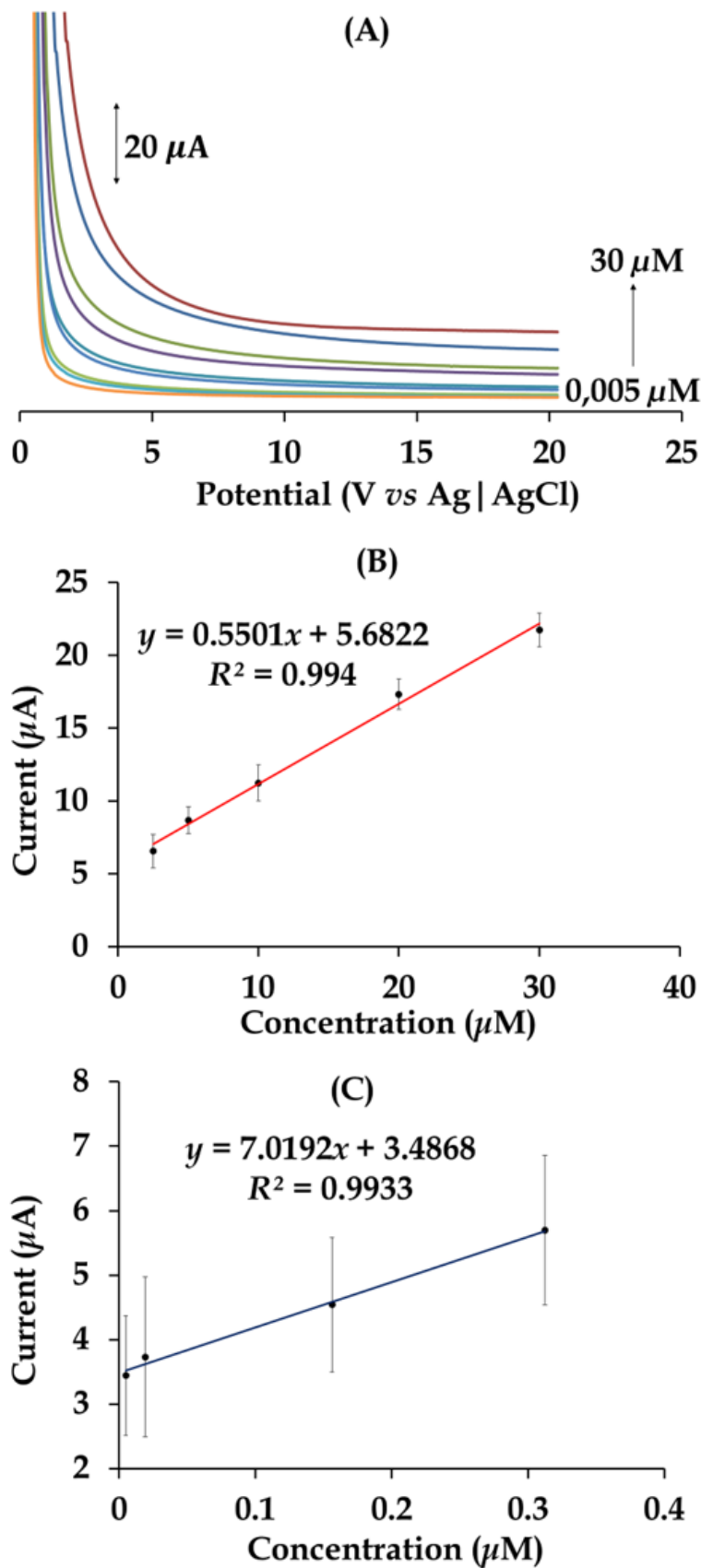


Figure 10. (A) Chronoamperograms recorded using CoPc-cou-f-MWCNTs/Naf-5/Pt placed in different concentrations of NVP prepared in PBS (pH=12). Calibration curves for the current response against (B) high and (C) low NVP concentrations.

Table 3. Comparison of NVP detection limits and linear ranges of various CMEs.

Electrode	Detection method	Linear range	Limit of detection (μM)	Reference
AuNPs/p(MB)/MWCNTs/GCE	DPASV	0.1-50 μM	0.056	[16]
Ura/CPE	DPV	0.1-70 μM	0.05	[22]
CuO-CNPs-GCE	LSV	0.1-100 μM	0.066	[12]
TiO ₂ /GNR/GCE	DPV	0.020-0.14 μM	0.043	[14]
Ag-PtNPs/MWCNTs/GCE	DPV	0.76-3.81 μM	0.021	[38]
Pd@rGO/MoS ₂ QDs GCE	DPV	0.1-80 μM	0.05	[39]
CP-Bi ₂ O ₃	DPV	0.050-50 μM	0.110	[40]
Hg/GCE	ASV	0.01-0.14 ppm	0.003	[41]
CoPc-cou- <i>f</i> -MWCNTs/Naf-5/Pt	LSV CA	0.0006-30 μM 0.004-0.3125 μM 2.5-30 μM	0.0002 0.00021	This work

AuNPs/p(MB)/f-MWCNTs: Gold nanoparticles/poly methylene blue/functionalized multiwalled carbon nanotubes

Ura/CPE: Uracil/carbon paste electrode

CuO-CNPs: Copper oxide-carbon nanoparticles

TiO₂/GNR: Titanium oxide/graphene nanoribbons

Ag-PtNPs/MWCNTs: Silver-platinum nanoparticles/multiwalled carbon nanotubes

Pd@rGO/MoS₂ QDs: Palladium at reduced graphene oxide/molybdenum disulfide quantum dots

CP-Bi₂O₃: Carbon paste-bismuth(III) oxide.

Hg: Thin film layer of mercury

3.8 Interference studies

To evaluate the selectivity of CoPc-cou-*f*-MWCNTs/Naf-5/Pt, different organic molecules, including ascorbic acid (AA), cysteine, dopamine (DA), metronidazole (MB) and uric acid (UA), were tested for potential signal suppression of NVP under the optimized analysis conditions. Figure 11 shows the current response to NVP (10 μM) in the presence of a 100-fold excess concentration of each of the abovementioned interferents. Notably, the NVP oxidation peak is more intense and better resolved than those of the interferents and appears at a lower positive oxidation potential compared to the solution without interferences (Figure 9A). The higher sensitivity and selectivity of CoPc-cou-*f*-MWCNTs/Naf-5/Pt compared to the investigated interferents could be ascribed to a higher affinity for the Naf-5 constituents because of electrostatic attractions between the N atoms of NVP and the cationic exchange sites of Naf-5. The aforementioned intermolecular interactions may be enhanced by hydrogen bonding

between the hydrogen of the amine group of the analyte and the coumarin groups of the CoPc molecules and carboxylic acid groups of the *f*-MWCNTs.

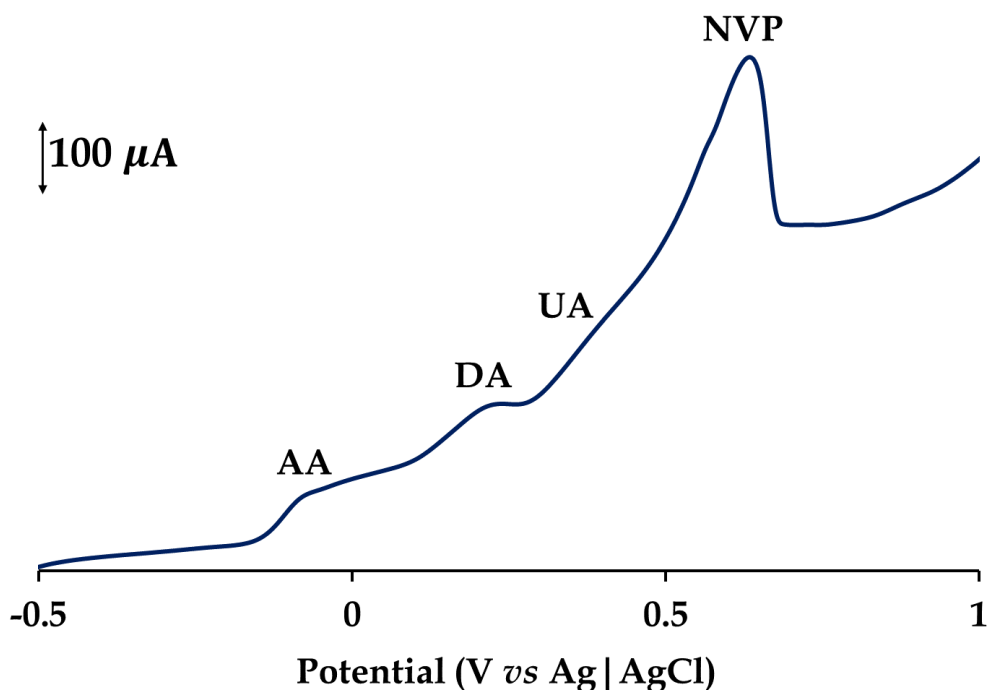


Figure 11: LSV obtained using CoPc-cou-*f*-MWCNTs/Naf-5/Pt placed in a sample matrix containing 10 μM NVP and 100 μM dopamine, uric acid, metronidazole, cysteine, and ascorbic acid prepared in PBS (pH = 12) solution.

3.9 LSV determination of NVP in prespiked and equilibrated river-water spiked samples

LSV was used to test the practicability of CoPc-cou-*f*-MWCNTs/Naf-5/Pt for the determination of NVP in a river-water sample collected from the Msunduzi River at the Camps Drift site in the city of Pietermaritzburg based in the Province of KwaZulu-Natal of the Republic of South Africa. The river-water sample (500 cm^3) was filtered, a phosphate buffer tablet was added, and the pH was adjusted to 12. The sample was prespiked with NVP to a final concentration of 1.75 μM . Several aliquots (10 cm^3) of the prespiked river water sample and an unspiked duplicate were left to age at room temperature for one day. There was no discernible current response for LSV of the unspiked duplicate river water sample using CoPc-cou-*f*-MWCNTs/Naf-5/Pt, indicating that the NVP concentration in the river water was below the LOD. A measurable current response for NVP was obtained for the prespiked (1.75 μM NVP) and equilibrated river-water samples. Subsequently, aliquots with incrementally larger volumes of 2.00, 4.00, 6.00 and 8.00 cm^3 of the 2.5 μM NVP standard were transferred to 4 x 10 cm^3 portions of the 10.00- cm^3 prespiked and pre-equilibrated river-water samples. The LSV current responses of the spiked samples are shown in Figure 12A. The calibration curve for the standard addition of NVP to the prespiked river water obtained using CoPc-cou-*f*-MWCNTs/Naf-5/Pt is presented in Figure 12B. The slope, the volume of the river-water aliquots and the concentration of the NVP standard solution were

used to estimate the NVP concentration of the prespiked water to be $1.88 \mu\text{M}$, which translates to a 110% recovery by the developed sensor.

The reproducibility of fabrication of CoPc-cou-*f*-MWCNTs/Naf-5/Pt was tested by analyzing a river-water sample spiked with $30 \mu\text{M}$ NVP by the LSV method. Five CoPc-cou-*f*-MWCNTs/Naf-5/Pt CMEs were prepared, and the LSV responses to the NVP signal were recorded. The percent relative standard deviation (%RSD) in measurements carried out using the five reproduced CMEs was found to be 4.2. Thus, the sensing film of the CoPc-cou-*f*-MWCNTs/Naf-5 Pt electrode used for the electrocatalytic oxidation of NVP in river water could be reproduced with good precision. The reproducibility of the CME was tested by recording the linear sweep currents for river water prespiked with $30 \mu\text{M}$ NVP for 6 consecutive runs using one of the fabricated CMEs. The %RSD for the currents was found to be 4.6. Consequently, it can be concluded that the fabricated CME demonstrated good reproducibility for measuring the NVP concentration in river-water samples.

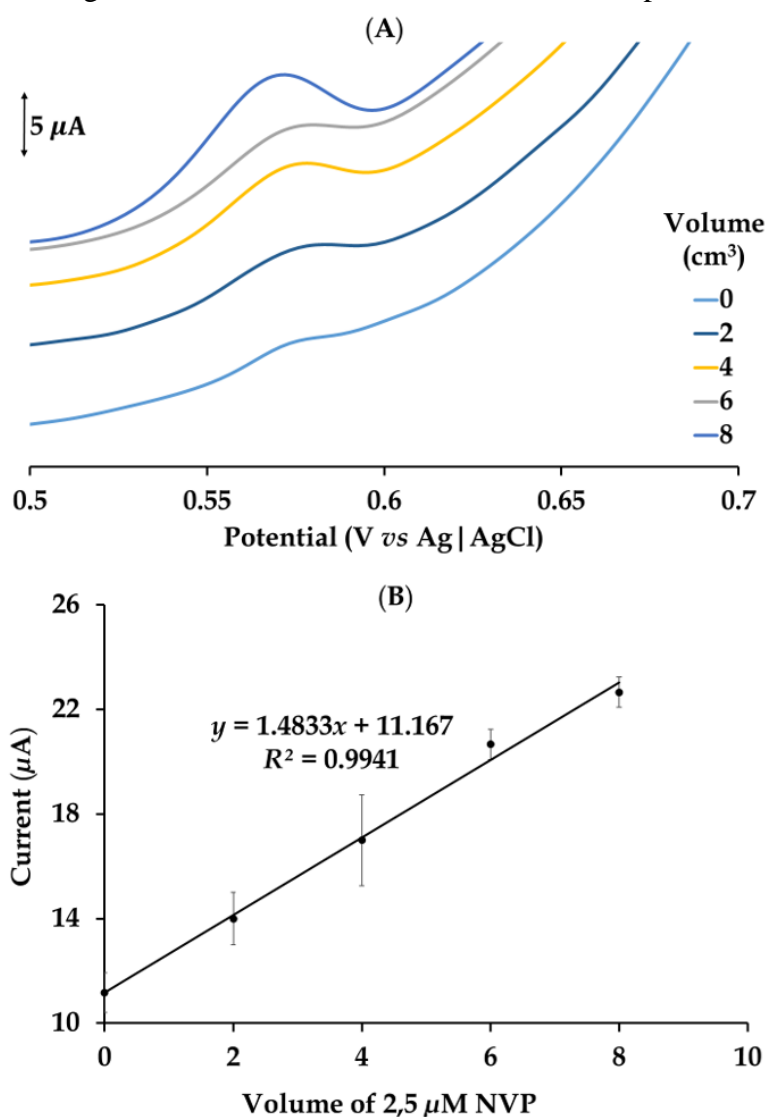


Figure 12:(A) LSV responses obtained using CoPc-cou-*f*-MWCNTs/Naf-5/Pt placed in 10.00 cm^3 of river water prespiked with $1.75 \mu\text{M}$ NVP after the addition of 2.00, 4.00, 6.00 and 8.00 cm^3 of a $2.5 \mu\text{M}$ NVP calibration standard. (B) Standard addition plot.

4. CONCLUSIONS

A durable and sensitive CoPc-cou-*f*-MWCNTs/Naf-5/Pt sensor for the catalytic oxidation of NVP was successfully fabricated by sequential drop casting of a suspension of CoPc-cou and *f*-MWCNTs, followed by immobilization of a drop of Naf-5. Under optimized conditions, CoPc-cou-*f*-MWCNTs/Naf-5/Pt showed lower detection limits than other investigated NVP electrochemical sensors. Linear sweep voltammetry results showed that CoPc-cou-*f*-MWCNTs/Naf-5/Pt detected NVP over a relatively broad linear concentration range (0.0006–30 μM), whereas the corresponding showed two linear ranges of detection (0.004–0.3125 μM and 2.5–30 μM) were identified using chronoamperometry. Furthermore, the detector showed excellent discrimination capabilities against selected common organic interferents present in matrixes. A recovery of 110% was obtained for LSV detection of NVP in a Msunduzi River water sample prespiked with 1.75 μM NVP. In addition, the potential of the CME for performing analytical qualitative and quantitative analyses of NVP in surface water samples was demonstrated. All the electroanalytical measurements made using the CME were highly repeatable, demonstrating the practicability of the CME.

ACKNOWLEDGMENTS

This study was funded by the National Research Foundation (NRF) of South Africa, Grant Number 111740, and the University of KwaZulu-Natal. The views expressed are those of the authors and should not be attributed to the NRF or University of KwaZulu-Natal.

References

1. B. Bozal, B. Uslu, S.A. Özkan, *Int J Chem Sci*, 2011 (2011) 1.
2. V.R. Kumar, B.P.B. Reddy, B.R. Kumar, K. Sreekanth, K.N. Babu, *J. Chromatogr. B*, 921-922 (2013) 9.
3. A.A. Castro, A.I.P. Cordoves, P.A.M. Farias, *Analytical Chemistry Insights*, 8 (2013) 21.
4. UNAIDS, 2019, 25-04-2021, <https://www.unaids.org/en/regionscountries/countries/southafrica>.
5. C. Swanepoel, H. Bouwman, R. Pieters, C. Bezuidenhout, Presence, concentrations and potential implications of HIV-anti-retrovirals in selected water resources in South Africa, in, Water Research Commission of South Africa, 2015, <http://www.wrc.org.za/wp-content/uploads/mdocs/2144-1-14.pdf>
6. O.A. Abafe, J. Späth, J. Fick, S. Jansson, C. Buckley, A. Stark, B. Pietruschka, B.S. Martincigh, *Chemosphere*, 200 (2018) 660.
7. C. Rimayi, D. Odusanya, J.M. Weiss, J. de Boer, L. Chimuka, *Science of the Total Environment*, 627 (2018) 1008.
8. M. Safari, M. Shamsipur, P. Zohrabi, H. Ebrahimzadeh, *Journal of Pharmaceutical and Biomedical Analysis*, 166 (2019) 95.
9. N.L. Rezk, R.R. Tidwell, A.D.M. Kashuba, *J. Chromatogr. B*, 774 (2002) 79.
10. M. Vogel, N. Bertram, J.C. Wasmuth, J. Emmelkamp, J.K. Rockstroh, C. Reichel, *Journal of Chromatographic Science*, 48 (2010) 91.
11. M. Rangapriya, N.N. Rajendran, *International Journal of Pharma Sciences and Research*, 5 (2014) 656.
12. S. Shahrokhian, R. Kohansal, M. Ghalkhani, M.K. Amini, *Electroanalysis*, 27 (2015) 1989.
13. N.L. Teradal, J. Seetharamappa, *Electroanalysis*, 27 (2015) 2007.

14. D. Apath, M. Moyo, M. Shumba, *Journal of Chemistry*, 2020, <https://doi.org/10.1155/2020/3932715>
15. P. Tiwari, N.R. Nirala, R. Prakash, *ChemistrySelect*, 3 (2018) 5341.
16. M.B. Gholivand, E. Ahmadi, M. Haseli, *Analytical Biochemistry*, 527 (2017) 4.
17. S. Massumi, E. Ahmadi, A. Akbari, M.B. Gholivand, *J. Electroanal. Chem.*, 876 (2020) 114508.
18. K. Kantize, I.N. Booyesen, A. Mambanda, *J. Electroanal. Chem.*, 850 (2019) 113391.
19. Ç.C. Koçak, A. Nas, H. Kantekin, Z. Dursun, *Talanta*, 184 (2018) 452.
20. J.P. Winiarski, M.R. de Barros, G.S. Wecker, G.R. Nagurniak, R.L.T. Parreira, R.F. Affeldt, R.A. Peralta, C.L. Jost, *Journal of Materials Chemistry C*, 8 (2020) 6839.
21. T.T. Guaraldo, L.A. Goulart, F.C. Moraes, M.R.V. Lanza, *Applied Surface Science*, 470 (2019) 555.
22. Y. Fan, J.H. Liu, H.T. Lu, Q. Zhang, *Colloids Surf. B. Biointerfaces*, 85 (2011) 289.
23. S. Chohan, I.N. Booyesen, A. Mambanda, M.P. Akerman, *J. Coord. Chem.*, 68 (2015) 1829.
24. C.D. Vecitis, M.H. Schnoor, M.S. Rahaman, J.D. Schiffman, M. Elimelech, *Environmental Science & Technology*, 45 (2011) 3672.
25. G. Yang, F. Zhao, *Biosensors and Bioelectronics*, 64 (2015) 416.
26. E. Ahmadi, M.B. Gholivand, *Analytical Methods*, 11 (2019) 4659.
27. T. Mugadza, T. Nyokong, *Polyhedron*, 30 (2011) 1820.
28. M. Shumba, S. Centane, F. Chindeka, T. Nyokong, *J. Electroanal. Chem.*, 791 (2017) 36.
29. S. Chohan, I.N. Booyesen, A. Mambanda, M.P. Akerman, *Inorg. Chim. Acta*, 447 (2016) 183.
30. S.C.B. Oliveira, A.M. Oliveira-Brett, *Electrochimica Acta*, 55 (2010) 4599.
31. N. Sekar, R.P. Ramasamy, *J. Microb. Biochem. Technol.* S, 6 (2013) 86.
32. X-Z Yuan, Y.C. Song, H. Wang, J. Zhang, EIS Equivalent Circuits, *In Electrochemical impedance spectroscopy in PEM Fuel Cells*, Springer, (2010), 139-192.
33. T. Mugadza, Y. Arslanolu, T. Nyokong, *Electrochimica Acta*, 68 (2012) 44.
34. V. Ngwenya, I.N. Booyesen, A. Mambanda, *J. Coord. Chem.*, 72 (2019) 1131.
35. H. Daneshinejad, M.A. Chamjangali, N. Goudarzi, A. Roudbari, *Materials Science and Engineering: C*, 58 (2016) 532.
36. M.K. Kumar, R.V. Prataap, S. Mohan, S.K. Jha, *Microchimica Acta*, 183 (2016) 1759.
37. I.A. Akinbulu, S. Khene, T. Nyokong, *Thin Solid Films*, 519 (2010) 911.
38. F.O. Okumu, B. Silwana, M.C. Matoetoe, *Electroanalysis*, 32 (2020) 3000.
39. P. Tiwari, N.R. Nirala, R. Prakash, *ChemistrySelect*, 3 (2018) 5341.
40. N.L. Teradal, J. Seetharamappa, *Electroanalysis*, 27 (2015) 2007.
41. A.A. Castro, R.Q. Aucelio, N.A. Rey, E.M. Miguel, P.A.M. Farias, *Combinatorial Chemistry & High Throughput*, 14 (2011) 22